ARTICLE

Special Issue on Invited Contributions from Award Winners of the 22nd National Electrochemical Congress in 2024

Entropy of Metal/Solution Interfaces: Thermodynamic Framework, Theoretical Models, and Roles of Interfacial Water

Zeng-Ming Zhang[a,b,#], Zi-Xi Liang[a,c,#], Jun Huang[a,b,*]

[a]Institute of Energy Technologies, IET-3: Theory and Computation of Energy Materials, Forschungszentrum Jülich GmbH, 52425 Jülich, Germany
[b]Faculty of Georesources and Materials Engineering, RWTH Aachen University, Aachen 52062, Germany
[c]Institute for a Sustainable Hydrogen Economy, INW-1, Forschungszentrum Jülich GmbH, 52425 Jülich, Germany

Abstract

Entropy is a basic thermodynamic property of the electrical double layer (EDL) at metal/solution interfaces, yet, its definition, measurement, and theoretical treatment are dispersed in the literature, and, in some cases, ambiguous. In this paper, we revisit the thermodynamic theory of EDL, from which two variants of entropy, excess entropy and formation entropy, are obtained and compared. In terms of the formation entropy, two calculation routes are validated in the context of a primitive EDL model, namely, the Gouy-Chapman (GC) model. After clarifying the concepts and calculation routes, we investigate interfacial water effects on the EDL entropy, using a refined Gouy-Chapman-Stern (GCS) model accounting for chemical potential difference between oxygen- and hydrogen-down water molecules, denoted $\delta\mu$. The model-derived differential capacitance and entropy are compared with experimental data for the EDL at Au(111) in an aqueous electrolyte solution. The model reveals that the charge of maximum entropy (CME) is negative when water molecules have higher tendency to take oxygen-down configuration at the uncharged surface. Moreover, the formation entropy profile becomes asymmetric around the CME, when $\delta\mu$ is potential-dependent. However, the model fails to simultaneously reproduce capacitance and entropy measurements on the same system taken from two separate studies, indicating deficiencies of the model or experimental errors. Nevertheless, this work stresses the importance of measuring both capacitance and entropy of EDLs at the same time.

Keywords: Electrical double layer; Excess entropy; Formation entropy; Interfacial water; Charge of maximum entropy

1. Introduction

Electrified metal-solution interfaces are central to a wide range of electrochemical and related technologies, including energy storage, electrosynthesis, and corrosion. The nanoscale interfacial structure formed at the boundary between a metal electrode and an electrolyte solution is named electrical double layer (EDL). Electronic charge on the electrode is screened by ionic and dipolar charge in the solution in the EDL. The EDL structure governs key interfacial properties such as capacitance, entropy and crucial local reaction conditions. Despite over a century of investigation, fundamental understanding of metal-solution interfaces remains an active research area [1, 2].

With growing interest in microscopic insights, thermodynamic, macroscopic studies fell out of fashion. However, a check of thermodynamic consistency is important for microscopic studies. Among the thermodynamic quantities, entropy is relatively more subtle [3]. In general terms, it quantifies how distribution of electrons, ions and solvent molecules in the EDL respond to temperature change [4, 5].

Received 13 November 2025; Received in revised form 10 December 2025; Accepted 24 December 2025
Available online 24 December 2025

#Contributed equally to this work as the co-first authors.
*Corresponding Author, E-mail: ju.huang@fz-juelich.de (J. Huang).

https://doi.org/10.61558/2993-074X.3601
1006-3471/© 2026 Xiamen University and Chinese Chemical Society. This is an open access article under the CC BY 4.0 license (https://creativecommons.org/licenses/by/4.0/).

Understanding the entropy of the EDL is thus instrumental for probing molecular orientation, ion packing, and phase transitions at interfaces. Moreover, entropy is directly connected to practical phenomena such as electrochemical heating and energy dissipation in devices operating at high frequencies [6–8].

A look into the literature on interfacial entropy shows a few notable issues. On the one hand, we have found several variants of entropy that could confuse the modeling and measurement of interfacial entropy. Definitions such as "surface excess entropy" and "entropy of formation" refer to related but different thermodynamic properties [3, 9]. On the other hand, a complete understanding of experimental capacitance and entropy data on "simple" EDLs at Au and Ag in weakly specifically adsorbing electrolytes is yet to come [10–14]. Moreover, the calculation of entropy in experimental and theoretical studies is sometimes inconsistent, hindering comparison between experiments and theory.

Early measurements on entropy in the context of electrochemistry could date back to 1941 when Lee and Tai estimated single ion entropies through the temperature dependence of the electrocapillary maximum of mercury. Randles and Whiteley revisited ion entropy measurements in 1956, and commented that Lee and Tai have neglected the temperature dependence of the inner potential difference between bulk mercury and bulk aqueous solution, which is closely related to the EDL entropy [15]. Subsequent research in the following decades continued revolving around mercury electrodes and was mainly based on the electrocapillary equation at constant pressure P [16],

$$-\mathrm{d}\gamma = \Gamma_s \mathrm{d}T + \sigma_\mathrm{M}\mathrm{d}E^{\pm} + \Gamma_{\pm}\mathrm{d}\mu, \tag{1}$$

where γ is the interfacial tension, σ_M is the surface charge density, $E^{\pm}$ stands for the electrode potential versus a reference electrode reversible to cations (+) or anions (–), μ is the chemical potential of the salt and $\Gamma_{\pm}$ for the effective surface excess of ions [17]. Γ_s is called **surface excess entropy**, which is defined as,

$$\Gamma_s = -\left(\frac{\partial\gamma}{\partial T}\right)_{P,E^{\pm},\mu}. \tag{2}$$

The surface excess entropy Γ_s could also be derivated from the cross-differentiation,

$$\left(\frac{\partial\Gamma_s}{\partial\sigma_\mathrm{M}}\right)_{P,\mu,T} = -\left(\frac{\partial E^{\pm}}{\partial T}\right)_{\sigma_\mathrm{M},P,m}, \tag{3}$$

from which Γ_s can be obtained by integrating the right-hand side with respect to the surface charge density σ_M, and the integration constant can be determined by a separate experiment under the condition of $\sigma_\mathrm{M} = 0$, i.e., the electrocapillary maximum for mercury electrode.

In 1973, Harrison *et al*. proposed the concept of the **entropy of formation of the interface** [17], which represents the difference in entropy of the components when present at the interface and in the bulk of the adjoining phases,

$$\Delta S_\mathrm{dl} = S^{\sigma} - m_\mathrm{M}^{\sigma}\overline{S}_\mathrm{M} - m_\mathrm{w}^{\sigma}\overline{S}_\mathrm{w} - m_{+}^{\sigma}\overline{S}_{+} - m_{-}^{\sigma}\overline{S}_{-}. \tag{4}$$

where superscript σ indicates the interfacial area. S^{σ} represents the total entropy of the interface. m_i^{σ} and $\overline{S}_\mathrm{i}$ represent the number of moles and partial molar entropies of the species concerned, respectively. The subscripts M, w, and i denote metal, water, and ions, respectively.

The main difference between the excess entropy Γ_s and the entropy of formation ΔS_dl lies in the contribution of ions. Harrison *et al*. pointed out that for a 1:1 electrolyte, the two types of entropy have the following relationship [17],

$$\Delta S_\mathrm{dl} = \Gamma_s - \Gamma_{-}\overline{S}_{-} - \Gamma_{+}\overline{S}_{+}. \tag{5}$$

Later, Garcia-Araez *et al*. [14] proved that the entropy of formation could also be derived from the cross-differentiation by introducing a Legendre transformation,

$$\left(\frac{\partial\Delta S_\mathrm{dl}}{\partial\sigma_\mathrm{M}}\right)_{P,m,T} = -\left(\frac{\partial\Delta\phi_\mathrm{S}^{\mathrm{M}}}{\partial T}\right)_{P,m,\sigma_\mathrm{M}}, \tag{6}$$

where $\Delta\phi_\mathrm{S}^{\mathrm{M}}$ is the inner potential difference between the solution bulk and metal (electrode) bulk.

Once the temperature coefficient of the potential change at the interface is evaluated, the formation entropy of the interface can be calculated from integration over the surface charge density, up to a constant of integration,

$$\begin{aligned}\Delta\Delta S_\mathrm{dl} &= \Delta S_\mathrm{dl}(\sigma_\mathrm{M}) - \Delta S_\mathrm{dl}(\sigma_\mathrm{M}=0)\\ &= -\int_0^{\sigma_\mathrm{M}}\left(\frac{\partial\Delta\phi_\mathrm{S}^{\mathrm{M}}}{\partial T}\right)_{P,m,\sigma_\mathrm{M}}\mathrm{d}\sigma.\end{aligned} \tag{7}$$

We refer to Eq. (7) as the "potential coefficient route".

Earlier measurements on mercury [18, 17] suggest that the formation entropy of EDL typically follows a parabolic profile with respect to surface charge density, but the detailed behavior depends on the solvent. Subsequent advances in instrumentation and single-crystal electrode preparation have enabled the measurements of differential EDL capacitance on well-defined surfaces, such as Pt(111) [14] and Au(210) [11]. One is possible to calculate EDL formation entropy from a set of EDL capacitance curves at different temperatures using Eq. (7).

Currently, understanding of the experimental entropy data remains semi-quantitative. Current focus is put on understanding characteristic potentials of entropy, notably the potential of maximum entropy (PME) [19], which refers to the electrode potential where the disorder (entropy) of solvent molecules at an electrochemical interface reaches its highest value. Experimental techniques such as laser-induced potential transient (LIPT) have been employed to measure PME. Early PME studies using the LIPT method on noble metal electrodes (e.g., Au) revealed that the PME generally lies near the potential of zero free charge (PZFC) but does not always coincide with it due to specific adsorption processes [10]. In the work of Ganassin *et al*., PME values for Ir(111) were systematically determined across pH 1–4 using LIPT and CO displacement methods [20]. A linear increase in the PME with pH (~30 mV per unit, vs. RHE) was reported. The PME on Ir(111) was consistently lower than on Pt(111), attributed to Ir's higher oxophilicity and, therefore, stronger interaction with OH^- and water molecules [20].

While PME is measured in experiments, the charge of maximum entropy (CME) is more frequently studied in theoretical works, primarily because it is easier to simulate the EDL under constant-charge conditions. Schwarz and colleagues have investigated microscopic origin of CME using molecular dynamics (MD) simulations [21]. Their work reveals that the CME is closely linked to solvent orientation at the interface. For example, at silver-water interfaces, the CME is negative (–5.8 μC·cm^{-2}) due to the preferential orientation of water molecules with oxygen atoms facing the electrode, while in acetonitrile, the CME is positive (–4.7 μC·cm^{-2}) as the acetonitrile group faces the electrode. These findings highlight the critical role of solvent-specific interactions in determining entropy asymmetry. However, challenges persist in achieving a consistent understanding of experimental data across metals. Specifically, both silver and gold possess negative charge of maximum entropy [10, 22], despite their distinct water adsorption properties: silver surface is hydrophilic while gold surface is more hydrophobic [23].

In this work, we contribute to addressing these challenges by clarifying two definitions of entropy, validating the equivalence of two approaches to calculate interfacial formation entropy, understanding experimental results across metals with an improved model of EDL.

The remainder of this paper is organized as follows. First, we introduce a refined EDL model that further considers potential-dependent, orientation-resolved chemisorption of water. Second, we review two routes of calculating interfacial formation entropy, and demonstrate their equivalence for a simple case. Third, we benchmark the model against experimental data, focusing on the origins of asymmetric entropy profiles and the negative charge of maximum entropy. The last section summarizes the findings and presents an outlook.

2. A Refined Model for Metal-Solution Interfaces

2.1. Considerations of the model

In this work, we adopt a recently modified GCS model highlighting the role of interfacial water molecules. In this model, the inner layer of EDL is further divided into two parts. One is the a closest approach plane (CAP) denoting the inner plane of the first-layer water molecules closest to the electrode surface, and the other one is the adsorbed solvent plane (ASP) denoting the outer plane of adsorbed solvent (water) molecules [24]. The outer Helmholtz layer (OHP) denotes the central plane of nonspecifically adsorbed ions, as shown in Fig. 1(a). Beyond the OHP, the diffuse layer forms out of the balance between electrostatic attraction and thermal motion of ions in the solution. Unlike the compact inner layer (or the Stern layer), the diffuse layer is characterized by a looser distribution of counterions to screen the surface charge.

A key task of EDL modeling is to determine the potential distribution across the metal-electrolyte interface [25]. Based on the scheme of Guidelli and Schmickler [26], we decompose the overall potential difference from the bulk metal (ϕ_M) to the bulk solution (ϕ_S) into,

$$\phi_M - \phi_S = \chi_M + \Delta\phi_{free} + \Delta\phi_{ad} + \Delta\phi_W, \tag{8}$$

in which χ_M denotes the potential drop at the metal surface due to electron distribution, which is usually treated as a constant [24], $\Delta\phi_{ad}$ the potential change due to partially charged, chemisorbed ions, $\Delta\phi_W$ the potential change due to orientational polarization of adsorbed water molecules, and $\Delta\phi_{free}$ the potential difference due to the free surface charge.

In this study, as specific ionic adsorption on the electrode surface is not considered, we neglect $\Delta\phi_{ad}$ and simplify Eq. (8) to,

$$\phi_M - \phi_S = \chi_M + \Delta\phi_{free} + \Delta\phi_W. \tag{9}$$

When the diffuse layer is described using a modified Poisson-Boltzmann theory considering finite ion sizes and the spaces between various layers are described as planar capacitors, we obtain $\Delta\phi_{free}$ as,

$$\Delta\phi_{free} = \mathrm{sign}(\sigma_{free})\frac{2RT}{F} \times \mathrm{arsinh}\left[\sqrt{\frac{1}{2\gamma}\left(\exp\left(\frac{\gamma}{2}\left(\frac{F\lambda_D\sigma_{free}}{RT\varepsilon_b}\right)^2\right)-1\right)}\right] + \sigma_{free}\sum_{i=1,2,3}\frac{\delta_i}{\varepsilon_i}, \tag{10}$$

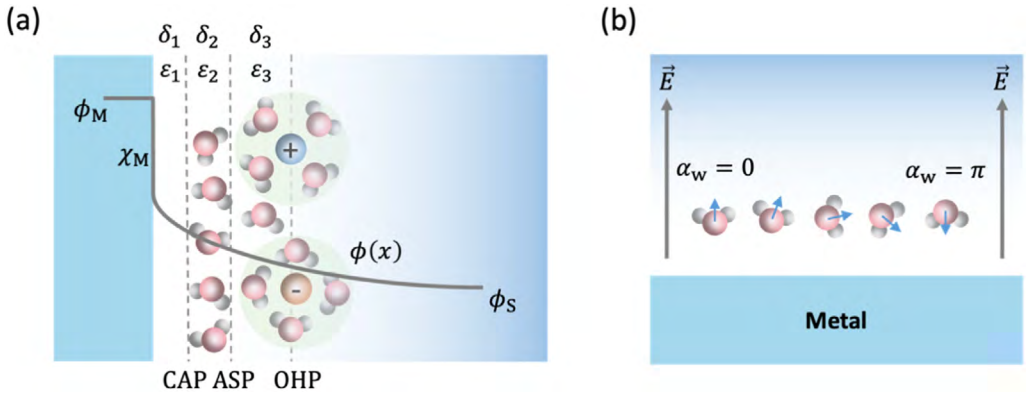


Fig. 1. (a) Schematic diagram of the EDL structure, composed of a closest approach plane (CAP) denoting the inner plane of the first-layer water molecules, outer adsorbed solvent plane (ASP) denoting the outer plane of the first-layer water molecules, and an OHP denoting the central plane of nonspecifically adsorbed ions. (b) A schematic diagram of water molecules within the ASP with a continuous spectrum of orientational states. Chemical metal-water interactions and electric field together determine the water dipole angle α_w, which denotes the angle between water dipoles and the outward electric field.

where the first term denotes the potential variation across the diffuse layer [27] and the second term is the potential variation across the space between various layers. σ_{free} denotes the free surface charge, which is equal to the total surface charge σ_{M} in the absence of specific adsorption [28], ε_{b} is the dielectric permittivity of the bulk solution, λ_{D} is the Debye length, which is defined as,

$$\lambda_{\text{D}} = \sqrt{\frac{\varepsilon_{\text{b}} RT}{2c_{\text{b}} F^2}}, \tag{11}$$

where c_{b} is the bulk ion concentration, $\gamma = 2c_{\text{b}} d_{\text{h}}^3$ with d_{h} being the diameter of hydrated ions.

The term $\Delta\phi_{\text{W}}$ accounts for the potential difference due to the average dipole moment of the first-layer water molecules [24], which can be calculated as,

$$\Delta\phi_{\text{W}} = -\frac{N_{\text{ad}}\theta_{\text{W}}\mu_{\text{W}}\langle\cos\alpha_{\text{W}}\rangle}{\varepsilon_2}. \tag{12}$$

The variable N_{ad} is the number of adsorption sites, θ_{W} is the coverage of water molecules, μ_{W} is the dipole moment of a water molecule, ε_2 the dielectric constant, and $\langle\cos\alpha_{\text{W}}\rangle$ is the statistical average of the angle function $\cos(\alpha_{\text{W}})$ with α_{W} being the angle between water dipoles and the outward electric field as shown in Fig. 1(b). $\langle\cos\alpha_{\text{W}}\rangle$ is a function of the chemical potential difference between the H-up ($\alpha_{\text{W}} = 0°$) and the H-down ($\alpha_{\text{W}} = \pi$) configurations, denoted as $\delta\mu$,

$$\langle\cos\alpha_{\text{W}}\rangle = -\coth\left(\frac{\mu_{\text{w}}E_{\text{loc}} + \delta\mu}{k_{\text{B}}T}\right) + \frac{k_{\text{B}}T}{\mu_{\text{w}}E_{\text{loc}} + \delta\mu}. \tag{13}$$

The variable E_{loc} in the formula is the average electric field due to σ_{free},

$$E_{\text{loc}} = -\frac{\sigma_{\text{M}}}{\varepsilon_2}. \tag{14}$$

Eq. (14) is consistent with the definition that water molecules prefer the O-down (H-up) configuration when $\delta\mu < 0$.

In experiments, the potential of the working electrode is controlled relative to a reference electrode. When the reference electrode (RE) and the working electrode (WE) are made of the same material, the electrode potential can be expressed as,

$$E = \phi_{\text{M}} - \phi_{\text{RE}} = (\phi_{\text{M}} - \phi_{\text{S}}) - (\phi_{\text{RE}} - \phi_{\text{S}}), \tag{15}$$

where ϕ_{RE} represents the inner potential of the reference electrode, which is in general case defined up to a constant that accounts for the difference in the work function between the working electrode and reference electrode materials. $(\phi_{\text{RE}} - \phi_{\text{S}})$ denotes the potential difference between the RE and the electrolyte solution. When the reversible hydrogen electrode (RHE) is employed as the reference electrode, the potential difference between the electrode and the solution is given by [24],

$$(\phi_{\text{M}} - \phi_{\text{S}}) = E_{\text{RHE}} + (\phi_{\text{RE}} - \phi_{\text{S}})_{\text{RHE}}. \tag{16}$$

The subscript 'RHE' specifies the reference electrode. According to the Nernst equation, the potential difference of the RHE can be related to the standard hydrogen electrode (SHE) by,

$$(\phi_{\text{RE}} - \phi_{\text{S}})_{\text{RHE}} = (\phi_{\text{RE}} - \phi_{\text{S}})_{\text{SHE}} - (\ln 10)\frac{RT}{F}\text{pH}. \tag{17}$$

Combining Eq. (16) and Eq. (17), we can obtain,

$$(\phi_{\text{M}} - \phi_{\text{S}}) = E_{\text{RHE}} + (\phi_{\text{RE}} - \phi_{\text{S}})_{\text{SHE}} - (\ln 10)\frac{RT}{F}\text{pH}, \tag{18}$$

or, equivalently,

$$\left(\phi_{\mathrm{M}}-\phi_{\mathrm{S}}\right)=E_{\mathrm{SHE}}+\left(\phi_{\mathrm{RE}}-\phi_{\mathrm{S}}\right)_{\mathrm{SHE}}, \tag{19}$$

with,

$$E_{\mathrm{SHE}}=E_{\mathrm{RHE}}-\left(\ln 10\right)\frac{RT}{F}\mathrm{pH}. \tag{20}$$

The differential double-layer capacitance, C_{dl} is defined as,

$$C_{\mathrm{dl}}=\frac{\partial\sigma_{\mathrm{M}}}{\partial E}, \tag{21}$$

where the $\sigma_{\mathrm{M}}=\sigma_{\mathrm{free}}$ is obtained using Eq. (10).

2.2. Model parameterization for the Au(111)/aqueous solution interfaces

Recently, Zhen *et al*. [25] parameterized the model with experimental C_{dl} data and molecule dynamics (MD) simulation data in literature. The parameters of the EDL model include permittivity ε_i of different layers and the thickness δ_i (i = 1, 2, 3) of them. Since an electron tail exists in the gap layer, ε_1 should exceed the vacuum permittivity ε_0. Herein, we set $\varepsilon_1=10\varepsilon_0$ to encompass the influence of electron spillover. For the Au(111) system, Li *et al*. determined the gap layer thickness to be ~1.5 Å through *ab initio* molecular dynamics (AIMD) simulations, so we have $\delta_1=1.5$ Å [29]. Previous studies by Li *et al*. and Xu *et al*. reported the distance between the first water layer and Au(111) surface to be 3~4 Å [30]. In our simulation, we employ an averaged value 3.5 Å and thus determine $\delta_2=2$ Å. Meanwhile, Parsons [31] and Bockris *et al*. [32] reported $\varepsilon_2=7.5\varepsilon_0$ and $\varepsilon_3=35\varepsilon_0$, respectively. For the space between ASP and OHP, we use $\delta_3=3$Å, corresponding to the typical radius of hydrated ions.

Regarding water molecules on ASP, we consider three key parameters: coverage of water molecules θ_{w}, μ_{w} and $\delta\mu$. The DFT computation of Domínguez-Flores *et al*. [33] revealed comparable water layer coverages (~0.55) across Au, and Ag surfaces. In our framework, we adopt $\theta_{\mathrm{w}}=0.55$ for Au(111). For the dipole moment μ_{w}, we use the intrinsic value of a water molecule $\mu_{\mathrm{w}}=1.85$ D [34]. The study of Schnur *et al*. [23] obtained adsorption energies of −0.41 eV and −0.43 eV for H-up and H-down configurations at Au(111). Therefore, we adopt the chemical potential difference ($\delta\mu_0$ = 1 k_{B}T) between H-down and H-up water configurations for Au(111). This indicates the hydrophobic character of the surface, with hydrogen atoms closer to the neutral electrode surface, that is, in an H-down configuration at zero surface charge.

With the parameterization, we now examine the simulated results from the previous model and assess their agreement with experimental observations. Zhen *et al*. [25] compared their model with experimental measurements reported by Adnan *et al*. [35]. Fig. 2 provides a comparison of C_{dl} between model and experiment at varying ionic concentrations. The C_{dl} profiles exhibit a pronounced asymmetry, with the anodic peak being higher than the cathodic one. This disparity primarily arises from the net preferential orientation of water molecules in H-down configurations ($\alpha_{\mathrm{W}}=\pi$) at an uncharged Au(111) surface. This interface has a larger capability of screening the positive surface charge, which tends to rotate water molecules toward the H-up orientation, resulting in a higher anodic capacitance peak, as discussed in a previous study [36].

Although the model reproduces the experimental trends reasonably well, it predicts lower capacitance values across the entire potential range for different ionic concentrations. In particular, the potential and magnitude of the anodic capacitance peak differ noticeably from the model-based values, arising likely from physical effects not captured in the present model. One key approximation is that the chemical potential difference $\delta\mu$ is treated as potential-independent. In reality, an applied potential modifies the extent of electron spillover and the metal's surface electronic structure, likely introducing potential dependence in $\delta\mu$. Additional factors, such as field-induced changes in the permittivity and thickness of the inner layer, namely, electrostriction [37], and specific adsorption of anions may also play a role. Analysis in the following section indicates that incorporating potential-dependent $\delta\mu$ can indeed elevate the anodic capacitance peak.

2.3. Potential-dependent water chemisorption

Previous AIMD studies by Braunwarth *et al*. on Pt(111) quantitatively demonstrated that variations in electrode potential alter the coverage of different oriented water molecules on the electrode surface [38]. Specifically, the coverage of water molecules with H-down configuration varies from around 0.2 to 0.7 when the applied potential increases from 0.5 V to 0.9 V [38]. Later, Le *et al*. revealed that the adsorption energy of H-up configuration water molecules changes with applied potential – as the applied potential increases from 0 to 2 V, the total adsorption energy decreases from around –0.05 eV to around –0.13 eV [36]. The computational results suggest that progressively positive electrode potentials stabilize H-up water orientations at the interface, causing quantifiable change in the total adsorption free energy for water molecules

Table 1. Model parameters of the simulation.

Symbol	Value	Significance
	Constants	
k_B (J·K^{-1})	1.38 ×10^{-23}	Boltzmann constant
e_0(C)	1.6 ×10^{-19}	Elementary charge
N_A (mol^{-1})	6.02 ×10^{-23}	Avogadro constant
F (C·mol^{-1})	96485	Faraday constant
h (J·s^{-1})	6.626 ×10^{-34}	Planck constant
ε_0 (F·m^{-1})	8.85 ×10^{-12}	Vacuum permittivity
ε_b (F·m^{-1})	78.5ε_0	permittivity of bulk water
T(K)	298	Temperature
$\delta\mu_0(k_BT)$	1	Water molecule chemical potential difference at pzc
θ_w	0.55	Coverage of adsorbed water molecules
	Au(111)-aqueous $HClO_4$ solution interfaces	
ε_1 (F·m^{-1})	10ε_0	permittivity between the electrode and the CAP
ε_2(F·m^{-1})	7.5ε_0	permittivity between the CAP and the ASP
ε_3(F·m^{-1})	35ε_0	permittivity between ASP and the OHP
δ_1 (Å)	1.5	thickness between the electrode and the CAP
δ_2 (Å)	2	thickness between the CAP and the ASP
δ_3 (Å)	3	thickness between ASP and the OHP
N_{ad}(m^{-2})	1.39 ×10^{19}	number of adsorption sites
$E^0_{pzc,SHE}$	0.30	potential of zero free charge when $\delta\mu = 0$
μ_w(C·m)	1.85D	water molecule dipole moment

with different orientations. It is worth mentioning that the total adsorption free energy differs from $\delta\mu$ in this model. While the total adsorption free energy includes electrostatic and chemical components, and the $\delta\mu$ term represents exclusively the difference in the chemical component. Therefore, if we assume that $\delta\mu$ becomes more negative at more positive potentials, chemical interactions also stabilize the O-down (H-up) configuration, in line with electrostatic interactions. Based on this, a general expression for $\delta\mu$ can be formulated as,

$$\delta\mu = f\left(E_M - E^0_{pzc,SHE}\right). \quad (22)$$

We employ a linear relationship between $\delta\mu$ and the electrode potential by introducing a first-order Taylor expansion,

$$\delta\mu = \delta\mu_0 + \beta_W\left(E_M - E^0_{pzc,SHE}\right) + o\left(E_M - E^0_{pzc,SHE}\right), \quad (23)$$

where $E^0_{pzc,SHE}$ is the potential of zero charge (PZC) defined as the value for the case of $\delta\mu$ = 0. β_W is a coefficient that characterizes the potential-dependent chemical potential difference of water with a unit $1\frac{k_BT}{V} = 2.57\times10^{-2}\,e_0$.

Fig. 3 illustrates the influences of $\delta\mu_0$ and β_W on the C_{dl} profiles. When $\beta_W = 0$, $\delta\mu_0 = -1\,k_BT$ and $\delta\mu_0 = 1\,k_BT$ correspond to water molecules preferentially adopting the H-up and H-down configurations, respectively, at zero surface charge, as shown in the inset of Fig. 3(a). For $\delta\mu_0 = -1\,k_BT$, the potential drop caused by the preferred H-up water configuration partially compensates the potential drop at the metal surface, resulting in a more negative E_{pzc}. The magnitude of the cathodic peak becomes larger because water molecules have a higher capability to screen negative surface charge by reorienting from the H-up

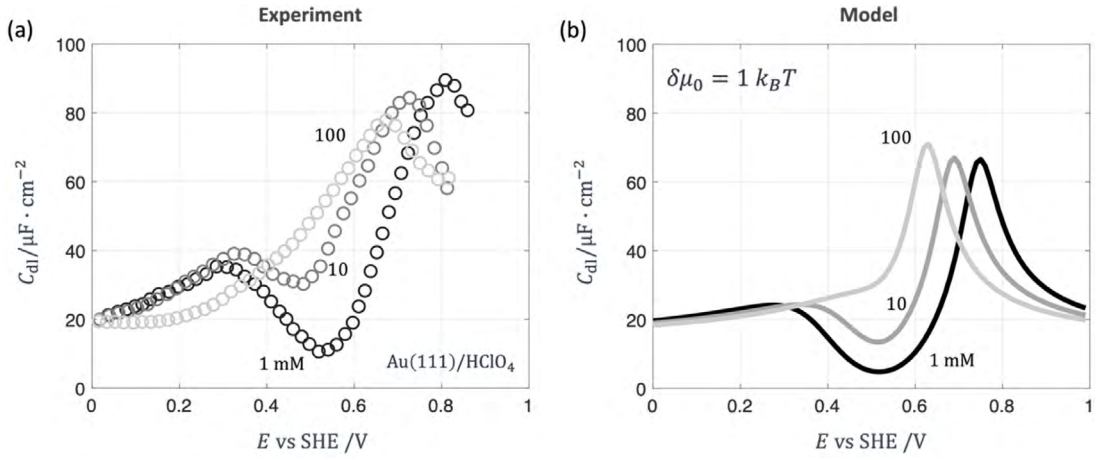


Fig. 2. Comparison of C_{dl} between (a) experiment and (b) model. The circles are the experimental results measured by Adnan et al. [35] and the lines are calculated using the model developed by Zhen et al. [25] where the chemical potential difference between H-up ($\alpha W = 0°$) and H-down ($\alpha W = \pi$) configurations is $\delta\mu_0 = 1\ k_BT$.

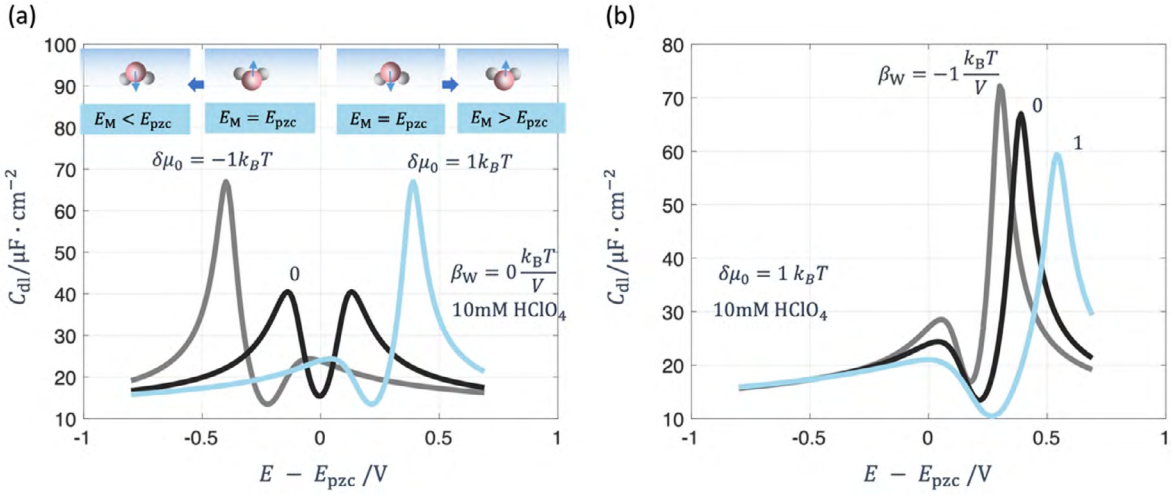


Fig. 3. Effect of potential-dependent chemical potential difference of water on C_{dl} for the cases of (a) $\beta_W = 0\ \frac{k_BT}{V}$, $\delta\mu_0 = -1, 0, 1\ k_BT$ and (b) $\delta\mu_0 = 1\ k_BT$. $\beta_W = -1, 0, 1\ \frac{k_BT}{V}$, $1\ \frac{k_BT}{V} = 4.11 \times 10^{-21}$ C = 0.0257 e_0. All other parameters are listed in Table 1.

to the H-down configuration than to screen positive surface charge. In contrast, for $\delta\mu_0 = 1\ k_BT$, the preferred H-down water configuration induces an additional potential drop, leading to a more positive E_{pzc}. The magnitude of the anodic peak becomes larger because water molecules more effectively screen positive surface charge by reorienting from the H-down to the H-up configuration than they do for negative surface charge, as shown in Fig. 3(a). These trends are consistent with our previous results [24, 25]. We further consider the effect of potential-dependent water chemisorption, namely, using nonzero $\beta_W \neq 0$ in the model. For the case of $\delta\mu_0 = 1\ k_BT$, a negative β_W decreases $\delta\mu$ at $E_M > E^0_{pzc,SHE}$, resulting in a smaller E_{pzc} and a larger anodic peak of C_{dl}, as shown in Fig. 3(b).

2.4. Theoretical framework and calculation of interfacial entropy

2.4.1. Detailed derivation of potential coefficient route

Following the research of Garcia-Araez *et al.* [14], we develop the thermodynamic framework of interfacial entropy specifically for an interface of an electrode in an aqueous $HClO_4$ solution. The starting point is the Gibbs equation for an electrochemical interface under constant pressure conditions,

$$-\mathrm{d}\gamma = \sum_i \Gamma_i \mathrm{d}\tilde{\mu}_i + \Gamma_S \mathrm{d}T, \tag{24}$$

where γ is the interfacial tension, Γ_i and $\tilde{\mu}_i$ are the Gibbs excess and electrochemical potential of species i, respectively. Γ_S is the entropy of the real system minus that of the ideal Gibbs system per unit surface, and T is the temperature.

Decomposing the first term on the right-hand side of Eq. (24) into contributions from the metal and solution phases, we obtain,

$$-\mathrm{d}\gamma = \sum_{\mathrm{i}}^{\mathrm{metal}} \Gamma_{\mathrm{i}}\mathrm{d}\tilde{\mu}_{\mathrm{i}} + \sum_{\mathrm{j}}^{\mathrm{sol}} \Gamma_{\mathrm{j}}\mathrm{d}\tilde{\mu}_{\mathrm{j}} + \Gamma_{\mathrm{S}}\mathrm{d}T, \tag{25}$$

where Γ_{i} and Γ_{j} are the mole numbers per unit surface area of species in the metal and the solution phase, respectively. The species i contains M, M^{z+},e^-. The species j contains H^+, OH^-, $\mathrm{H_2O}$, $\mathrm{ClO_4^-}$, assuming full dissociation of $\mathrm{HClO_4}$.

On the metal side, the metal atom can be treated as a phase composing of metal atoms, fully dissociated cationic cores and freely movable valence electrons. Then we have,

$$\begin{aligned}\sum_{\mathrm{i}}^{\mathrm{metal}} \Gamma_{\mathrm{i}}\mathrm{d}\tilde{\mu}_{\mathrm{i}} &= \Gamma_{\mathrm{M}}\mathrm{d}\mu_{\mathrm{M}} + \Gamma_{\mathrm{M}^{z+}}\mathrm{d}\tilde{\mu}_{\mathrm{M}^{z+}} + \Gamma_{\mathrm{e}^-}\mathrm{d}\tilde{\mu}_{\mathrm{e}^-} \\ &= \Gamma_{\mathrm{M}}\mathrm{d}\mu_{\mathrm{M}} + \Gamma_{\mathrm{M}^{z+}}\mathrm{d}\mu_{\mathrm{M}^{z+}} + \Gamma_{\mathrm{e}^-}\mathrm{d}\mu_{\mathrm{e}^-} \\ &+ (z_{\mathrm{M}}F\Gamma_{\mathrm{M}^{z+}} - F\Gamma_{\mathrm{e}^-})\mathrm{d}\phi_{\mathrm{M}} = \sum_{\mathrm{i=M,M^{z+},e^-}}^{\mathrm{metal}} \Gamma_{\mathrm{i}}\mathrm{d}\mu_{\mathrm{i}} + \sigma_{\mathrm{M}}\mathrm{d}\phi_{\mathrm{M}},\end{aligned} \tag{26}$$

where Γ_{e^-} and μ_{e^-} are the surface excess and chemical potential, respectively, of conduction electrons relative to the neutral bulk metal.

The solution part can be expanded into chemical and electrostatic terms,

$$\sum_{\mathrm{j}}^{\mathrm{sol}} \Gamma_{\mathrm{j}}\mathrm{d}\tilde{\mu}_{\mathrm{j}} = \sum_{\mathrm{j}}^{\mathrm{sol}} \Gamma_{\mathrm{j}}\mathrm{d}\mu_{\mathrm{j}} + \sum_{\mathrm{j}}^{\mathrm{sol}} z_{\mathrm{j}}F\Gamma_{\mathrm{j}}\,\mathrm{d}\phi_{\mathrm{S}}. \tag{27}$$

The charge of excess, nonspecifically adsorbed ions on the solution side (denotes as σ_{S}) can be expressed as,

$$\sigma_{\mathrm{S}} = \sum_{\mathrm{j}}^{\mathrm{sol}} z_{\mathrm{j}}F\Gamma_{\mathrm{j}}. \tag{28}$$

Since the interface is electroneutral, σ_{S} is equal in absolute value and opposite in sign to the metallic excess charge, that is,

$$\sigma_{\mathrm{S}} = -\sigma_{\mathrm{M}}. \tag{29}$$

The Gibbs equation Eq. (25) can be rewritten as,

$$\begin{aligned}-\mathrm{d}\gamma &= \sigma_{\mathrm{M}}\mathrm{d}\phi_{\mathrm{M}} - \sigma_{\mathrm{M}}\mathrm{d}\phi_{\mathrm{S}} + \sum_{\mathrm{i=M,M^{z+},e}}^{\mathrm{metal}} \Gamma_{\mathrm{i}}\mathrm{d}\mu_{\mathrm{i}} + \sum_{\mathrm{j}}^{\mathrm{sol}} \Gamma_{\mathrm{j}}\mathrm{d}\mu_{\mathrm{j}} + \Gamma_{\mathrm{S}}\mathrm{d}T \\ &= \sigma_{\mathrm{M}}\mathrm{d}\phi_{\mathrm{S}}^{\mathrm{M}} + \sum_{\mathrm{i=M,M^{z+},e}}^{\mathrm{metal}} \Gamma_{\mathrm{i}}\mathrm{d}\mu_{\mathrm{i}} + \sum_{\mathrm{j}}^{\mathrm{sol}} \Gamma_{\mathrm{j}}\mathrm{d}\mu_{\mathrm{j}} + \Gamma_{\mathrm{S}}\mathrm{d}T,\end{aligned} \tag{30}$$

where $\phi_{\mathrm{S}}^{\mathrm{M}} = \phi_{\mathrm{M}} - \phi_{\mathrm{S}}$ is the inner potential difference between the bulk metal and bulk solution.

In the metal bulk, the metal ions, atoms and electrons are in equilibrium, hence, we have,

$$\mu_{\mathrm{M}} = \mu_{\mathrm{M}^{z+}} + z_{\mathrm{M}}\mu_{\mathrm{e}^-}. \tag{31}$$

In the solution bulk, the equilibrium of water dissociation means,

$$\mu_{\mathrm{H_2O}} = \mu_{\mathrm{H}^+} + \mu_{\mathrm{OH}^-}. \tag{32}$$

The dependent variables, $\mu_{\mathrm{i}}\left(\mathrm{i} = \mathrm{M},\ \mathrm{M}^{z+},\mathrm{e}\right)$, can be eliminated through the Gibbs-Duhem equations for the metal phases.

Then, the Gibbs equation can be rewritten as,

$$\begin{aligned}-\mathrm{d}\gamma &= \sigma_{\mathrm{M}}\mathrm{d}\left(\Delta\phi_{\mathrm{S}}^{\mathrm{M}}\right) + (\Gamma_{\mathrm{H}^+} - \Gamma_{\mathrm{OH}^-})\mathrm{d}\mu_{\mathrm{H}^+} \\ &+ \left(\Gamma_{\mathrm{H_2O}} + \Gamma_{\mathrm{OH}^-}\right)\mathrm{d}\mu_{\mathrm{H_2O}} + \Gamma_{\mathrm{ClO_4^-}}\mathrm{d}\mu_{\mathrm{ClO_4^-}} + \Gamma_{\mathrm{S}}\mathrm{d}T,\end{aligned} \tag{33}$$

where we have used $\mathrm{d}\mu_{\mathrm{OH}^-} = -\mathrm{d}\mu_{\mathrm{H}^+}$. Detailed derivations of chemical potential terms, e.g., $\mathrm{d}\mu_{\mathrm{H_2O}}$, are presented in the Supporting Information.

The Gibbs equation in Eq. (33) can be rewritten as,

$$\begin{aligned}-\mathrm{d}\gamma &= \sigma_{\mathrm{M}}\mathrm{d}\left(\Delta\phi_{\mathrm{S}}^{\mathrm{M}}\right) \\ &+ \left(\Gamma_{\mathrm{S,H_2O}} - \Gamma_{\mathrm{H^+,H_2O}}\bar{S}_{\mathrm{H}^+} - \Gamma_{\mathrm{ClO_4^-,H_2O}}\bar{S}_{\mathrm{ClO_4^-}}\right)\mathrm{d}T,\end{aligned} \tag{34}$$

where $\bar{S}_{\mathrm{i}} = S_{\mathrm{i}} / n_{\mathrm{tot}}$ is the partial molar entropy, n_{tot} is the total mole of solution species. $\bar{S}_{\mathrm{sol}}$ is expressed as the sum of all contributions of the solution components,

$$\bar{S}_{\mathrm{sol}} = \chi_{\mathrm{H_2O}}\bar{S}_{\mathrm{H_2O}} + \chi_{\mathrm{OH}^-}\bar{S}_{\mathrm{OH}^-} + \chi_{\mathrm{H}^+}\bar{S}_{\mathrm{H}^+} + \chi_{\mathrm{ClO_4^-}}\bar{S}_{\mathrm{ClO_4^-}}. \tag{35}$$

where $\chi_{\mathrm{i}} = n_{\mathrm{i}} / n_{\mathrm{tot}}$ is mole fraction of species i.

For a constant solution composition and at constant pressure, the potential of components can be written as,

$$\mathrm{d}\mu_{\mathrm{i}} = -\bar{S}_{\mathrm{i}}\mathrm{d}T. \tag{36}$$

In Harrison's work, the entropy of formation of the interface is defined as the difference in the entropy of the elements when they are forming part of it and when they are present in the bulk of their respective phases,

$$\Delta S_{\mathrm{dl}} = \Gamma_{\mathrm{S}} - \Gamma_{\mathrm{OH}^-}\bar{S}_{\mathrm{OH}^-} - \Gamma_{\mathrm{H}^+}\bar{S}_{\mathrm{H}^+} - \Gamma_{\mathrm{ClO_4^-}}\bar{S}_{\mathrm{ClO_4^-}} - \Gamma_{\mathrm{H_2O}}\bar{S}_{\mathrm{H_2O}}. \tag{37}$$

Then, considering Eq. (33) and Eq. (34), we can rewrite the equation as,

$$\begin{aligned}\Delta S_{\mathrm{dl}} &= \Gamma_{\mathrm{S,H_2O}} + \left(\Gamma_{\mathrm{H_2O}} + \Gamma_{\mathrm{OH}^-}\right)\frac{\bar{S}_{\mathrm{sol}}}{\chi_{\mathrm{H_2O}}} - \left(\Gamma_{\mathrm{H_2O}} + \Gamma_{\mathrm{OH}^-}\right)\bar{S}_{\mathrm{H_2O}} \\ &- \Gamma_{\mathrm{ClO_4^-}}\bar{S}_{\mathrm{ClO_4^-}} - (\Gamma_{\mathrm{H}^+} - \Gamma_{\mathrm{OH}^-})\bar{S}_{\mathrm{H}^+}.\end{aligned} \tag{38}$$

Meanwhile, considering the situation that the number of water molecules is far greater than the number of OH^-, indicating $\chi_{\mathrm{H_2O}} >> \chi_{\mathrm{OH}^-}$. We then make the following approximation,

$$\Delta S_{\mathrm{dl}} \approx \Gamma_{\mathrm{S,H_2O}} - \Gamma_{\mathrm{H^+,H_2O}}\bar{S}_{\mathrm{H}^+} - \Gamma_{\mathrm{ClO_4^-,H_2O}}\bar{S}_{\mathrm{ClO_4^-}}. \tag{39}$$

The Parsons function is expressed as,

$$\xi = \sigma_{\mathrm{M}} \Delta\phi_{\mathrm{S}}^{\mathrm{M}} + \gamma. \tag{40}$$

Total differential of ξ leads to

$$\mathrm{d}\xi = \Delta\phi_{\mathrm{S}}^{\mathrm{M}} \mathrm{d}\sigma_{\mathrm{M}} - \Delta S_{\mathrm{dl}} \mathrm{d}T. \tag{41}$$

Eq. (41) leads to,

$$\left(\frac{\partial \Delta S_{\mathrm{dl}}}{\partial \sigma_{\mathrm{M}}}\right)_{\sigma_{\mathrm{M}},T,m} = -\left(\frac{\partial \Delta\phi_{\mathrm{S}}^{\mathrm{M}}}{\partial T}\right)_{\sigma_{\mathrm{M}},P,m}. \tag{42}$$

And finally, the formation entropy of the EDL can be obtained by,

$$\begin{aligned} \Delta\Delta S_{\mathrm{dl}} &= \Delta S_{\mathrm{dl}}(\sigma_{\mathrm{M}}) - \Delta S_{\mathrm{dl}}(\sigma_{\mathrm{M}} = 0) \\ &= -\int_0^{\sigma_{\mathrm{M}}} \left(\frac{\partial \Delta\phi_{\mathrm{S}}^{\mathrm{M}}}{\partial T}\right)_{\sigma_{\mathrm{M}},P,m} \mathrm{d}\sigma. \end{aligned} \tag{43}$$

In most previous studies, the formation entropy has been defined only up to an arbitrary constant and is therefore determined relative to a chosen reference state. Following common practice—and analogous to assigning a reference for the absolute electrochemical potential—we set the formation entropy of the uncharged interface as the reference, $\Delta S_{\mathrm{dl}}(\sigma_{\mathrm{M}} = 0)$. With this convention, the integration in Eq. (43) yields a well-defined quantity that we refer to as the relative formation entropy, meaning that its value is uniquely specified relative to the zero-charge state.

2.4.2. Free energy route

Alternatively, the formation entropy can be obtained directly from the Helmholtz free energy of the EDL. We term this the "free energy route". The Helmholtz free energy A of the EDL is defined as a spatial integral of the areal free energy density $a(x)$,

$$A = \int_0^{\infty} a(x) \mathrm{d}x, \tag{44}$$

where 0 denotes the metal surface, and ∞ the metal bulk.

While the free energy approach is general for any EDL model, we use the Gouy-Chapman (GC) model as an example to illustrate its basic idea. As for the GC model, the free energy density incorporates both electrostatic contributions and configurational entropy terms of the diffuse layer,

$$a(x) = -\frac{1}{2}\varepsilon_s \phi^2 + F\phi(c_+ - c_-) - T s_{\mathrm{conf}}, \tag{45}$$

where ε_s is the dielectric permittivity of the solution, ϕ is the local electrostatic potential, c_+ and c_- are the concentrations of positive and negative ions, respectively. The first and second terms correspond to the electrostatic energy stored in the EDL, while s_{conf} accounts for the volume density of configurational entropy. The formation entropy of the EDL can be then rewritten as,

$$\begin{aligned} \Delta\Delta S_{\mathrm{dl}}^{A} &= \left(\frac{\partial A}{\partial T}\right)_V \\ &= \int_0^{\infty} \frac{\partial}{\partial T}\left(-\frac{1}{2}\varepsilon_s \phi^2 + F\phi(c_+ - c_-) - T s_{\mathrm{conf}}\right) \mathrm{d}x, \end{aligned} \tag{46}$$

where the superscript A here indicates that the formation entropy is calculated from the Helmholtz free energy, and $s_{\mathrm{conf}}(x) = -k_B\left(n_+ \ln\frac{n_+}{n_{\mathrm{ref}}} + n_- \ln\frac{n_-}{n_{\mathrm{ref}}}\right)$ with n_{i} being the number density of particle i and n_{ref} the reference number density used to normalize the argument of the logarithm function [39].

2.5. Comparison of two calculation routes for the case of the Gouy-Chapman theory

The Gouy-Chapman theory is derived based on the Poisson-Boltzmann equation,

$$\nabla^2\phi(x) = -\frac{\rho(x)}{\varepsilon_s} = \sum_i -\frac{z_i F c_i(x)}{\varepsilon_s}, \tag{47}$$

where $\rho(x)$ is the charge density at distance x from the surface. In a 1:1 electrolyte system, $\rho(x)$ is given by,

$$\begin{aligned} \rho(x) &= F\left(c_0 \exp\left(-\frac{F\phi}{RT}\right) - c_0 \exp\left(\frac{F\phi}{RT}\right)\right) \\ &= -2Fc_0 \sinh\left(\frac{F\phi}{RT}\right). \end{aligned} \tag{48}$$

The boundary conditions are,

$$\phi(x=0) = \phi_0,\ \phi(x \to \infty) = 0, \tag{49}$$

where ϕ_0 is the electrode potential relative to the PZC.

The surface charge density σ_{M} is related to the local electric field at the interface,

$$\sigma_{\mathrm{M}} = -\varepsilon_s \left.\frac{\mathrm{d}\phi}{\mathrm{d}x}\right|_{x=0}. \tag{50}$$

We multiply both sides of Eq. (47) by $\frac{\mathrm{d}\phi}{\mathrm{d}x}$,

$$\frac{\mathrm{d}\phi}{\mathrm{d}x} \cdot \frac{\mathrm{d}^2\phi}{\mathrm{d}x^2} = \frac{2Fc_0}{\varepsilon_s} \sinh\left(\frac{F\phi}{RT}\right) \cdot \frac{\mathrm{d}\phi}{\mathrm{d}x}, \tag{51}$$

which is equivalent to,

$$\frac{1}{2} \cdot \mathrm{d}\left(\frac{\mathrm{d}\phi}{\mathrm{d}x}\right)^2 = \frac{2c_0 RT}{\varepsilon_s} \mathrm{d}\left(\cosh\left(\frac{F\phi}{RT}\right)\right). \tag{52}$$

Integrating Eq. (52) and using the boundary condition of $x \to \infty$, $\phi \to 0$, $\frac{\mathrm{d}\phi}{\mathrm{d}x} \to 0$, we obtain,

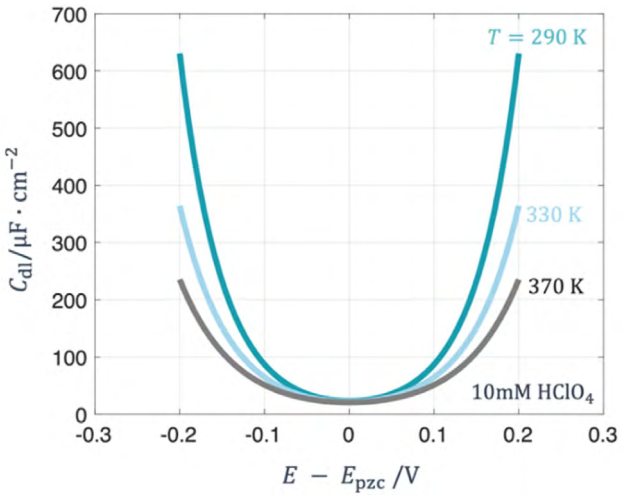


Fig. 4. Temperature effect on C_{GC} in 10 mmol·L^{-1} $HClO_4$ aqueous solution.

$$\frac{\mathrm{d}\phi}{\mathrm{d}x}=\sqrt{\frac{4c_0RT}{\varepsilon_s}\left(\cosh\left(\frac{F\phi}{RT}\right)-1\right)}. \tag{53}$$

At the electrode surface, $x=0$, we know $\phi=\phi_0$. Therefore, the surface charge density is given as,

$$\sigma_{\mathrm{M}}=-\varepsilon_s\left.\frac{\mathrm{d}\phi}{\mathrm{d}x}\right|_{x=0}=\frac{2\varepsilon_s RT}{F\lambda_{\mathrm{D}}}\sinh\left(\frac{F\phi_0}{2RT}\right). \tag{54}$$

Therefore, the differential double-layer capacitance is given by

$$C_{\mathrm{GC}}=\frac{\partial\sigma_{\mathrm{M}}}{\partial\phi_0}=\frac{\varepsilon_s}{\lambda_{\mathrm{D}}}\cosh\frac{F\phi_0}{2RT}, \tag{55}$$

where $\phi_0=E_{\mathrm{M}}-E_{\mathrm{pzc}}$.

The dependence of C_{GC} on temperature is presented in Fig. 4. An increase in temperature enlarges the Debye length λ_{D}, thereby reducing C_{GC}, as described by Eq. (55).

In the potential coefficient route, the procedure consists of three main steps. First, the relationship between the applied potential and E_{M} the surface charge density σ_{M} is calculated at a series of temperatures using Eq. (54), as shown in Fig. 5(a). Second, the corresponding coefficients $\left(\frac{\partial\Delta\phi_S^{\mathrm{M}}}{\partial T}\right)_{P,m,\sigma_{\mathrm{M}}}$ in Eq. (42) are determined, with the results presented in Fig. 5(b). Finally, the formation entropy is obtained from Eq. (43). In addition, the implementation code in MATLAB is provided in the Supporting Information for the sake of reproducibility.

The comparison of $\Delta\Delta S_{\mathrm{dl}}$ between the two calculation routes, in the context of the GC theory, is shown in Fig. 6. Consistent results are observed between the two routes. In the rest of this paper, the potential coefficient route, being computationally more efficient, is employed to calculate the formation entropy of the EDL.

2.6. Formation entropy from the refined EDL model

2.6.1. Effect of water adsorption on the formation entropy of EDL

The effect of water adsorption on C_{dl} at constant temperature has been analyzed in Section 2. In this section, we will investigate how variations in potential-dependent water chemisorption, tunned by β_{W}, influence the formation entropy of the EDL.

The formation entropy of the EDL considering the entropy of interfacial water molecules at zero surface charge is given by,

$$\Delta S_{\mathrm{dl}}=\Delta\Delta S_{\mathrm{dl}}+\Delta S_{\mathrm{W}}\left(\sigma_{\mathrm{M}}=0\right), \tag{56}$$

where ΔS_{W} is the entropy change of water molecules when they are moved from bulk solution to the ASP. In the present refined EDL model, the Helmholtz free energy of water molecules at the ASP is given by,

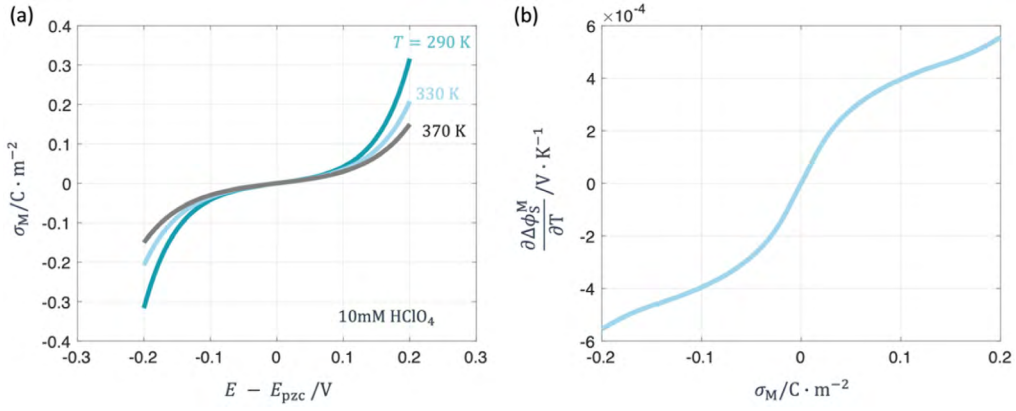


Fig. 5. Intermediate results of calculating the interfacial formation entropy based on GC model in 10 mmol·L^{-1} $HClO_4$ aqueous solution. (a) Temperature effect on the surface charge density profiles, (b) the potential coefficient $\left(\frac{\partial\Delta\phi_S^{\mathrm{M}}}{\partial T}\right)_{P,m,\sigma_{\mathrm{M}}}$ as a function of surface charge density.

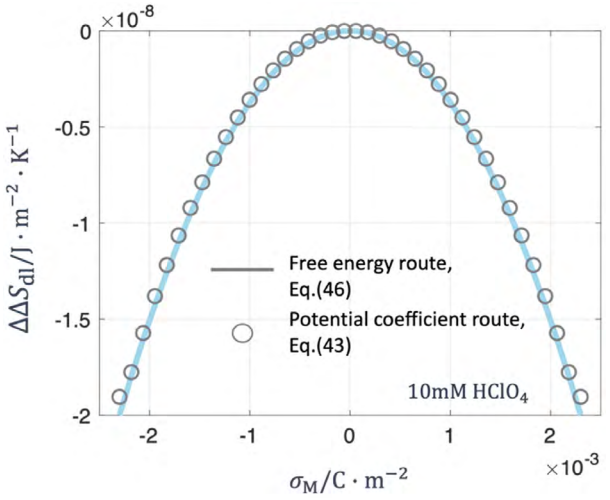


Fig. 6. Comparison of $\Delta\Delta S_{dl}$ between the potential coefficient route (circle) and free energy route (solid line) based on Gouy-Chapman theory. The electrolyte is a 10 mmol·L⁻¹ $HClO_4$ aqueous solution.

$$A_{\mathrm{W}} = -k_{\mathrm{B}}TN_{\mathrm{W}}\ln\left[\frac{\sinh(x)}{x}\right], \tag{57}$$

where N_{W} is the number of water molecules per unit area and $x = \delta\mu_0 / k_{\mathrm{B}}T$. Therefore, ΔS_{W} is a constant value given by,

$$\Delta S_{\mathrm{W}} = k_{\mathrm{B}}N_{\mathrm{W}}\ln\left[\frac{\sinh(x)}{x}\right] - k_{\mathrm{B}}N_{\mathrm{W}}\frac{\left[x\cdot\cosh(x)-\sinh(x)\right]}{\sinh(x)}. \tag{58}$$

Fig. 7(a) shows a systematic decrease in the model-calculated C_{dl} with increasing temperature. This trend arises from the temperature dependence of the Debye length (see Eq. (11)). The increased ionic kinetic energy at higher temperatures promotes greater spatial dispersion of ions, which increases the effective thickness of the EDL and consequently reduces C_{dl}. This behavior agrees with the temperature-dependent C_{GC} trend shown in Fig. 4.

Correspondingly, the temperature-dependent surface charge-potential relationship is presented in Fig. 7(b). The temperature effects in cathodic and anodic regions are identical for the case of $\delta\mu_0 = 0$, because water molecules adopt random orientations in the absence of electrostatic interactions, as discussed in Fig. 3.

The profile of the potential coefficient $\left(\frac{\partial\Delta\phi_{\mathrm{S}}^{\mathrm{M}}}{\partial T}\right)_{P,m,\sigma_{\mathrm{M}}}$ in Fig. 7(c) is symmetric as cations and anions are assumed to have the same size, resulting in a symmetric

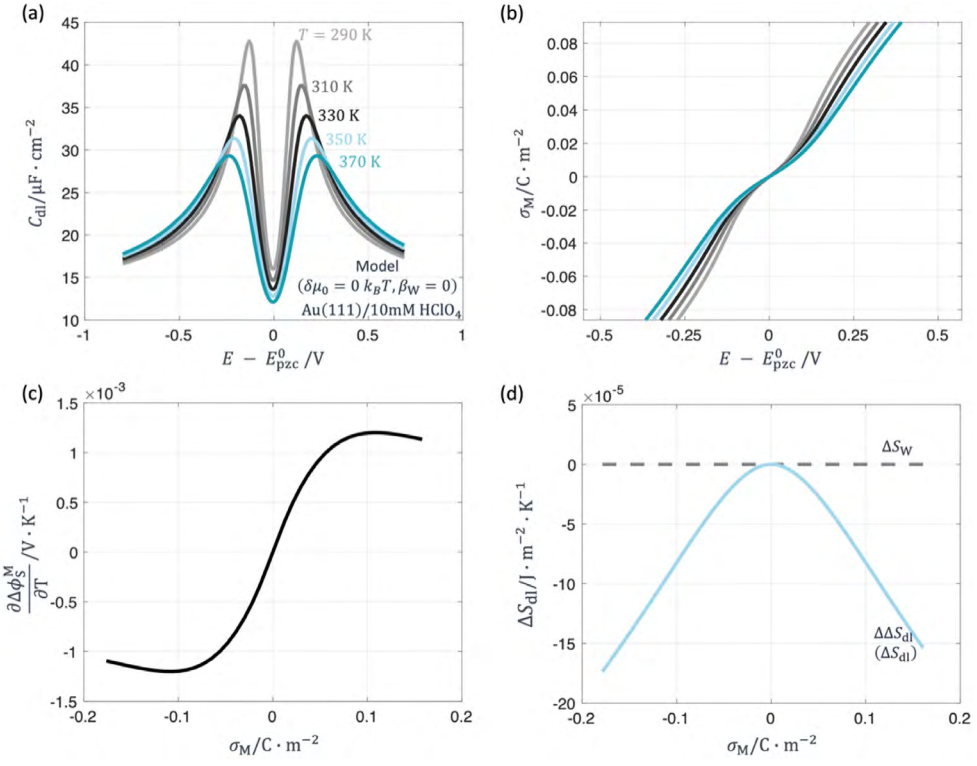


Fig. 7. Temperature effect on (a) C_{dl} and (b) surface charge density profiles in 10 mmol·L⁻¹ $HClO_4$ aqueous solution. (c) shows the potential coefficient $\left(\frac{\partial\Delta\phi_{\mathrm{S}}^{\mathrm{M}}}{\partial T}\right)_{P,m,\sigma_{\mathrm{M}}}$ and (d) the entropy change of water molecules, ΔS_{W}, the relative formation entropy of EDL, $\Delta\Delta S_{\mathrm{dl}}$, and the formation entropy, ΔS_{dl} for the case of $\delta\mu_0 = 0\ k_{\mathrm{B}}T$, $\beta_{\mathrm{W}} = 0\ \frac{k_{\mathrm{B}}T}{V}$. Other parameters are the same as those listed in Table 1.

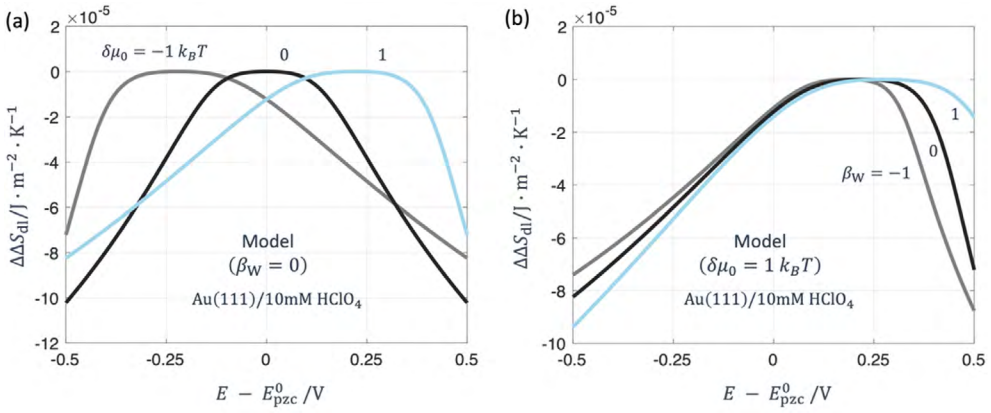


Fig. 8. Effect of potential-dependent chemical potential difference of water on $\Delta\Delta S_{dl}$. (a) Results for $\beta_W = 0$ and $\delta\mu_0 = -1, 0, 1\ k_BT$. (b) Results for $\delta\mu_0 = 1\ k_BT$ and $\beta_W = 0 -1, 0, 1 \frac{k_BT}{V}$. Other parameters are listed in Table 1.

bell-shaped profile of $\Delta\Delta S_{dl}$, as shown in Fig. 7(d). The zero value of ΔS_W in Fig. 7(d) arises from the use of $\delta\mu_0 = 0$. Consequently, ΔS_{dl} overlaps with $\Delta\Delta S_{dl}$.

After clarifying the procedure for calculating the interfacial formation entropy using the potential coefficient route, the effect of chemical potential difference of water on $\Delta\Delta S_{dl}$ is analyzed in Fig. 8. For the case of $\beta_W = 0$, the peak potential of the $\Delta\Delta S_{dl}$ profile, denoted as E_p^S, shifts toward more positive values when $\delta\mu_0 > 0$ and toward more negative values when $\delta\mu_0 < 0$. The positive (negative) shift of E_p^S, induced by the preferred H-down (H-up) water configuration, is consistent with the shift of E_{pzc}. The $\Delta\Delta S_{dl}(E)$ profile becomes steeper on the anodic side for $\delta\mu_0 > 0$ and on the cathodic side for $\delta\mu_0 < 0$, as shown in Fig. 8(a). This asymmetric behavior results from a larger change in consistent with the shift of when the water molecules are oriented from the H-down (H-up) to the H-up (H-down) configuration when $\delta\mu_0 > 0$ ($\delta\mu_0 < 0$). Furthermore, Fig. 8(b) illustrates the effect of a nonzero β_W ($\beta_W \neq 0$) on $\Delta\Delta S_{dl}(E)$ for the case of $\delta\mu_0 > 0$. A negative β_W decreases $\delta\mu$ at $E_M > E^0_{pzc,SHE}$, resulting in a more negative E_p^S and a steeper $\Delta\Delta S_{dl}(E)$ profile. These trends are consistent with the influences of $\delta\mu_0$ and β_W on the C_{dl} profile discussed in Section 2.

2.6.2. Comparison between model and experiment in dual lens of capacitance and entropy

Climent *et al*. [10] measured the interfacial entropy using the Laser-Induced Potential Transient (LIPT) method. In this approach, Au(111) electrodes immersed in 100 mmol·L^{-1} $HClO_4$ were subjected to pulsed laser heating, and the resulting open-circuit potential relaxation was analyzed to determine the formation entropy using the potential gradient route, as expressed in Eq. (43). Experimentally, $\Delta\Delta S_{dl}$ shows a nearly parabolic dependence on surface charge density, and the charge of maximum entropy (CME) appears at approximately −3 μC·cm^{-2}. We compare below model-derived C_{dl} and $\Delta\Delta S_{dl}$ with experimental data by tuning the key parameters, $\delta\mu_0$ and β_W.

For the base case we use $\delta\mu_0 = 1 k_BT$ according to AIMD simulations [23] and $\beta_W = -2, 0, 2\frac{k_BT}{V}$. With this parameter set, the anodic capacitance peak is higher than the cathodic peak, because water molecules are more capable to screen positive surface charge by reorienting from the average H-down configuration to an average H-up configuration, consistent with Fig. 3. Although semi-quantitatively reproducing experimental C_{dl}, the model gives a $\Delta\Delta S_{dl}$ profile with a positive CME. Maximum disorder in the water layer occurs when the preferred average H-down configuration is countered by the positive surface charge. This, however, contradicts the experimentally observed negative CME, as shown in Fig. 9(a, b).

To meet the negative CME, we use a negative $\delta\mu_0 = -0.5 k_BT$ in the second case where $\beta_W = 0, 1, 2\frac{k_BT}{V}$ is examined. For the case of $\beta_W = 0$, though the model reproduces the negative CME, $\Delta\Delta S_{dl}$ progressively deviates from experimental data at highly positive surface charge. In addition, a negative $\delta\mu_0$ results in a higher cathodic capacitance peak, which contradicts the experimental C_{dl}, as shown in Fig. 9(c, d). We further introduce the effect of potential-dependent water chemisorption, namely, using nonzero $\beta_W \neq 0$ in the model. A positive β_W decreases $\delta\mu$ to more a negative value at $E_M < E_{pzc}$, reducing the anodic C_{dl} peak. $\Delta\Delta S_{dl}$ aligns much more closely with experiment at $\beta_W = 2\frac{k_BT}{V}$. However, the model then deviates markedly from experimental C_{dl}.

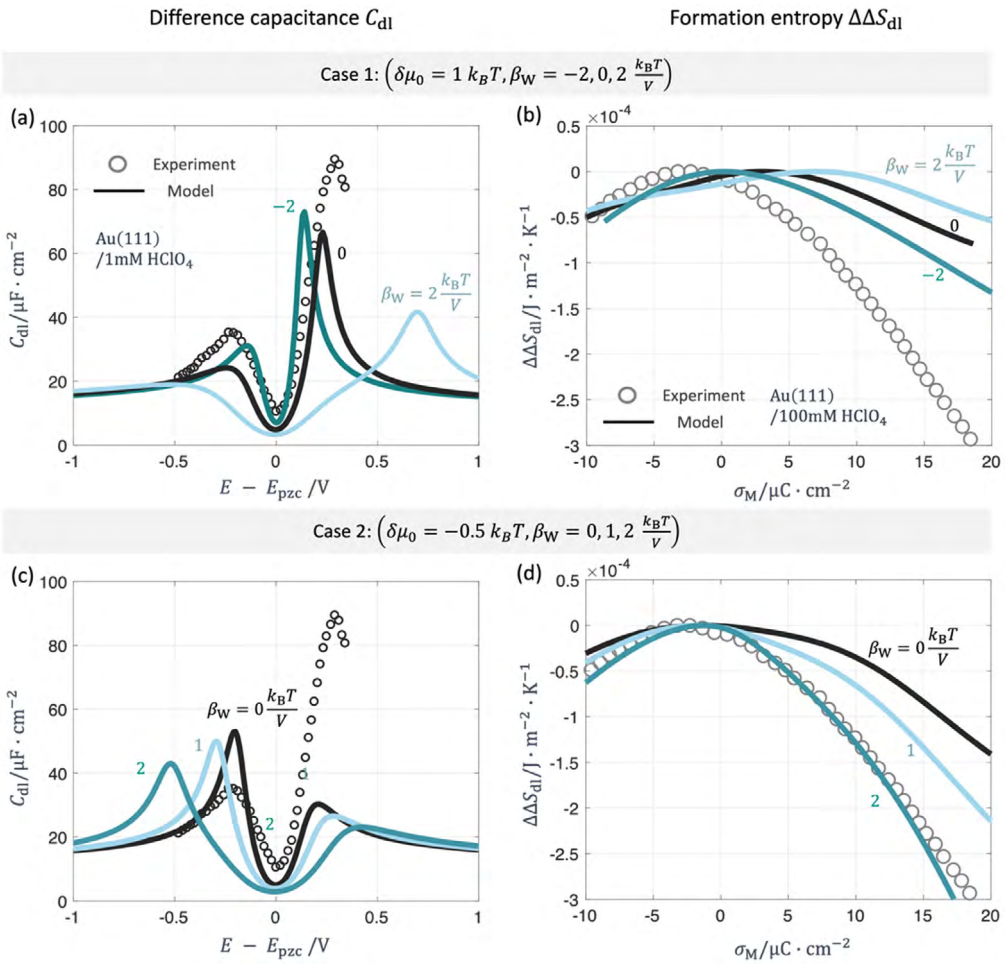


Fig. 9. Comparison of (a, c) C_{dl} and (b, d) $\Delta\Delta S_{dl}$ between model and experiment of Au(111)/$HClO_4$ solution. (a, b) For the case of $\delta\mu_0$ =1 k_BT, β_W = −2, 0, 2 $\frac{k_BT}{V}$, (c, d) for the case of $\delta\mu_0$ = −0.5 k_BT, β_W = 0, 1, 2 $\frac{k_BT}{V}$. Experimental C_{dl} data is taken from Adnan et al. [35] and $\Delta\Delta S_{dl}$ data is taken from Climent et al. [11]. Other parameters are the same as those listed in Table 1.

In summary, the model cannot simultaneously reproduce both capacitance and entropy measurements for the same system, indicating that certain physical effects are not fully captured by the model or there are inconsistencies between two separate experiments conducted in two different labs.

3. Conclusions and outlooks

In this work, we revisited entropy of metal-solution interfaces by establishing a rigorous thermodynamic framework that distinguishes between the excess entropy and the formation entropy. Two computational approaches—the potential coefficient route and the free energy route—were benchmarked for the case of Gouy-Chapman theory, demonstrating their equivalence. For the electric double layer, we developed an extended Gouy-Chapman-Stern model that explicitly incorporates potential-dependent chemical potential difference between oxygen- and hydrogen-down water molecules, denoted $\delta\mu$. The model is used to understand how C_{dl} and ΔS_{dl} are influenced by $\delta\mu$. Using a constant $\delta\mu$, the model correlates a higher anodic capacitance peak with a positive charge of maximum entropy. Introducing potential dependence of $\delta\mu$ changes the symmetry of both C_{dl} and ΔS_{dl}. However, the model cannot simultaneously reproduce both capacitance and entropy data for the EDL at Au(111) in $HClO_4$ aqueous solution. This mismatch indicates that key physical effects are not fully captured by the present model. Additionally, experimental uncertainties, such as ion specific adsorption and systematic errors between the two separate experimental studies, cannot be excluded. In the future, a refined treatment of solvent in the EDL, such as the temperature- and field-dependent permittivity, is needed to resolve the discrepancy. In addition, we expect to see systematic measurements

of both differential capacitance and formation entropy of Au single crystals as a function of electrolyte parameters in future.

Acknowledgments

This work was supported by the Initiative and Networking Fund of the Helmholtz Association (Grant No. VH-NG-1709), and European Research Council (ERC) Starting Grant (MESO-CAT, Grant agreement No. 101163405).

Conflict of interests

The authors declare no conflicts of interest.

Data availability

The data supporting the findings of this study can be obtained from the corresponding author upon a reasonable request.

Author contributions

Zeng-Ming Zhang: Writing – original draft, Investigation, Data curation, Validation, Conceptualization, Formal analysis. Zi-Xi Liang: Writing – original draft, Investigation, Data curation. Jun Huang: Supervision, Writing – Conceptualization, Formal analysis, review.

References

[1] Helmholtz H. Studien Über Electrische Grenzschichten[J]. Ann. Phys., 1879, 243(7): 337–382. https://doi.org/10.1002/andp.18792430702.

[2] Stern O H. Zur Theorie Der Elektrolytischen Doppelschicht. Z. Für Elektrochem[J]. Angew. Phys. Chem., 1924, 30(21–22): 508–516. https://doi.org/10.1002/bbpc.192400182.

[3] Guidelli R, Aloisi G, Leiva E, Schmickler W. Contribution to the entropy of formation of metal/solution interphases from metal electrons[J]. J. Phys. Chem., 1988, 92(23): 6671–6675. https://doi.org/10.1021/j100334a036.

[4] Conway B E. Electrochemical supercapacitors [M]. Springer US: Boston, MA, 1999. https://doi.org/10.1007/978-1-4757-3058-6.

[5] Schmickler W, Santos E. Interfacial electrochemistry [M]. Springer Berlin Heidelberg: Berlin, Heidelberg, 2010. https://doi.org/10.1007/978-3-642-04937-8.

[6] Bazant M Z, Kilic M S, Storey B D, Ajdari A. Towards an understanding of induced-charge electrokinetics at large applied voltages in concentrated solutions[J]. Adv. Colloid Interface Sci., 2009, 152(1–2): 48–88. https://doi.org/10.1016/j.cis.2009.10.001.

[7] Zeng L, Chen M, Wang Z X, Qiao R, Feng G. Structural evolution governs reversible heat generation in electrical double layers[J]. Phys. Rev. Lett., 2023, 131: 096201. https://doi.org/10.1103/PhysRevLett.131.096201.

[8] Garrick T R, Koch B J, Choi M, Du X N, Adeyinka A M, Staser J A, Choe S Y. Quantifying the entropy and enthalpy of insertion materials for battery applications via the multi-species, multi-reaction model[J]. J. Electrochem. Soc., 2024, 171(2): 23502. https://doi.org/10.1149/1945-7111/ad1d27.

[9] Trasatti S. Structure of the metal/electrolyte solution interface: New data for theory[J]. Electrochim. Acta, 1991, 36(11–12): 1659–1667. https://doi.org/10.1016/0013-4686(91)85023-Z.

[10] Climent V, Coles B A, Compton R G. Laser-induced potential transients on a Au(111) single-crystal electrode. Determination of the potential of maximum entropy of double-layer formation[J]. J. Phys. Chem. B, 2002, 106(20): 5258–5265. https://doi.org/10.1021/jp020054q.

[11] Hamelin A, Stoicoviciu L, Silva F. The temperature dependence of the doublelayer properties of gold faces in perchloric acid solutions: Part I. The (210) Gold Face[J]. J. Electroanal. Chem. Interfacial Electrochem., 1987 229(1–2): 107–214. https://doi.org/10.1016/0022-0728(87)85134-3.

[12] Hamelin A, Stoicoviciu L, Silva F. The temperature dependence of the double-layer properties of gold faces in perchloric acid solutions part II. The (110) gold face[J]. J. Electroanal. Chem. Interfacial Electrochem. 1987, 234: 93–105. https://doi.org/10.1016/0022-0728(87)87043-8.

[13] Hamelin A, Doubova L, Stoicoviciu L, Trasatti S. The temperature dependence of the double layer parameters of the (111) face of silver[J]. J. Electroanal. Chem. Interfacial Electrochem., 1988, 244(1–2): 133–145. https://doi.org/10.1016/0022-0728(88)80101-3.

[14] Garcia-Araez N, Climent V, Feliu J. Separation of temperature effects on double-layer and charge-transfer processes for platinum|solution interphases. entropy of formation of the double layer and absolute molar entropy of adsorbed hydrogen and OH on Pt(111)[J]. J. Phys. Chem. C, 2009, 113(46): 19913–19925. https://doi.org/10.1021/jp904638d.

[15] Randles J E B, Whiteley K S. The temperature dependence of the electrocapillary maximum of mercury[J]. Trans. Faraday Soc., 1956, 52: 1509. https://doi.org/10.1039/tf9565201509.

[16] Hills G J, Payne R. Temperature and pressure dependence of the double layer capacity at the mercury-solution interface[J]. Trans. Faraday Soc., 1965, 61: 326. https://doi.org/10.1039/tf9656100326.

[17] Harrison J A, Randles J E B, Schiffrin D J. The entropy of formation of the mercury-aqueous solution interface and the structure of the inner layer[J]. J. Electroanal. Chem. Interfacial Electrochem., 1973, 48(3): 359–381. https://doi.org/10.1016/S0022-0728(73)80369-9.

[18] Hills G J. Compact double layer as a function of temperature and pressure[J]. J. Phys. Chem., 1969, 73(11): 3591–3597. https://doi.org/10.1021/j100845a010.

[19] Fawcett W R. Liquids, solutions, and interfaces: From classical macroscopic descriptions to modern microscopic details [M]. Oxford University Press, 2004.

[20] Ganassin A, Sebastián P, Climent V, Schuhmann W, Bandarenka A S, Feliu J. On the pH dependence of the potential of maximum entropy of Ir(111) electrodes[J]. Sci. Rep., 2017, 7(1): 1246. https://doi.org/10.1038/s41598-017-01295-1.

[21] Sundararaman R, Schwarz K. Solvent effects determine the sign of the charges of maximum entropy and capacitance at silver electrodes[J]. J. Chem. Phys., 2023, 158(12): 121102. https://doi.org/10.1063/5.0143307.

[22] Doubova, Trasatti. The temperature coefficient of the potential of zero charge of Ag single crystal face electrodes in aqueous electrolyte solution[J]. Condens. Matter Phys., 2001, 4(4): 759. https://doi.org/10.5488/CMP.4.4.759.

[23] Schnur S, Groß A. Properties of metal-water interfaces studied from first principles[J]. New J. Phys., 2009, 11(12): 125003. https://doi.org/10.1088/1367-2630/11/12/125003.

[24] Huang, J. Zooming into the inner Helmholtz plane of Pt(111)–aqueous solution interfaces: Chemisorbed water and partially charged ions[J]. JACS Au, 2023, 3(2): 550–564. https://doi.org/10.1021/jacsau.2c00650.

[25] Zhen E F, Chen Y X, Huang J. double-layer capacitance peaks: Origins, ion dependence, and temperature effects[J]. J. Chem. Phys., 2025, 162(14): 144702. https://doi.org/10.1063/5.0251548.

[26] Schmickler W, Guidelli R. The partial charge transfer[J]. Electrochim. Acta, 2014, 127: 489–505. https://doi.org/10.1016/j.electacta.2014.02.057.

[27] Kornyshev A A. Double-layer in ionic liquids: Paradigm change?[J]. J. Phys. Chem. B, 2007, 111(20): 5545–5557. https://doi.org/10.1021/jp067857o.

[28] Zhang M K, Cai J, Chen Y X. On the Electrode charge at the metal/solution interface with specific adsorption[J]. Curr. Opin. Electrochem., 2022, 36: 101161. https://doi.org/10.1016/j.coelec.2022.101161.

[29] Li C Y, Le J B, Wang Y H, Chen S, Yang Z L, Li J F, Cheng J, Tian Z Q. *In situ* probing electrified interfacial water structures at atomically flat surfaces[J]. Nat. Mater., 2019, 18(7): 697–701. https://doi.org/10.1038/s41563-019-0356-x.

[30] Xu M L, Liu S H, Vijay S, Bligaard T, Kastlunger G. Benchmarking water adsorption on metal surfaces with Ab Initio molecular dynamics[J]. J. Chem. Phys., 2024, 160(24): 244707. https://doi.org/10.1063/5.0205552.

[31] Parsons R. The structure of the mercury-electrolyte interphase in the presence of thiourea[J]. Proc. A, 1961, 261(1304): 79–90. https://doi.org/10.1098/rspa.1961.0062.

[32] Bockris J O, Devanathan M A V, Müller K. On the structure of charged interfaces[J]. Electrochemistry, 1965, 832–863. https://doi.org/10.1016/B978-1-4831-9831-6.50068-0.

[33] Domínguez-Flores F, Kiljunen T, Groß A, Sakong S, Melander M M. Metal-water interface formation: Thermodynamics from Ab Initio molecular dynamics simulations[J]. J. Chem. Phys., 2024, 161(4): 44705. https://doi.org/10.1063/5.0220576.

[34] Gregory J K, Clary D C, Liu K, Brown M G, Saykally R J. The water dipole moment in water clusters[J]. Science, 1997, 275(5301): 814–817. https://doi.org/10.1126/science.275.5301.814.

[35] Adnan A, Behjati S, Félez-Guerrero N, Ojha K, Koper M T M. Tracking the surface structure and the influence of cations and anions on the double-layer region of a Au(111) electrode[J]. Phys. Chem. Chem. Phys., 2024, 26(32): 21419–21428. https://doi.org/10.1039/D4CP02133A.

[36] Lee J, Yeo H, Lee R G, Kim Y H. Ab Initio theory of the nonequilibrium adsorption energy[J]. Npj Comput. Mater., 2024, 10(1): 60. https://doi.org/10.1038/s41524-024-01242-5.

[37] Macdonald J R. Theory of the differential capacitance of the double layer in unadsorbed electrolytes[J]. J. Chem. Phys., 1954, 22(11): 1857–1866. https://doi.org/10.1063/1.1739933.

[38] Braunwarth L, Jung C, Jacob T. Potential-dependent Pt(111)/water interface: Tackling the challenge of a consistent treatment of electrochemical interfaces[J]. ChemPhysChem, 2023, 24(1): e202200336. https://doi.org/10.1002/cphc.202200336.

[39] Zhang L L, Li C K, Huang J. A beginners' guide to modelling of electric double layer under equilibrium, nonequilibrium and AC conditions[J]. J. Electrochem., 2022, 28(2): 2108471. https://doi.org/10.13208/j.electrochem.210847.

金属/溶液界面的熵：热力学框架、理论模型和界面水的作用

张增明[a,b,#], 梁子西[a,c,#], 黄俊[a,b,*]
[a]能源技术研究所, IET-3：能源材料理论与计算, 德国于利希研究中心, 德国 于利希, 52425
[b]亚琛工业大学地球资源与材料工程学院, 德国 亚琛, 52062
[c]可持续氢研究所, INW-1, 德国 于利希研究中心, 德国 于利希, 52425

摘要:

熵是金属/溶液界面双电层的基本热力学性质之一, 但其定义、测量方法和理论处理在现有文献中较为分散, 且在某些情况下仍存在歧义。本文重新审视了双电层的热力学理论, 明确区分并比较了两类熵：过剩熵和形成熵。针对形成熵, 在最基本的双电层模型-Gouy-Chapman (GC) 模型框架下, 验证了两种等价的计算途径。

在澄清相关概念和计算方法之后, 本文采用改进的 Gouy-Chapman-Stern (GCS) 模型研究了界面水对双电层形成熵的影响。该模型显式引入了氧端朝向与氢端朝向水分子之间的化学势差, 记为 $\delta\mu$。模型计算得到的微分电容和熵与 Au(111) 电极在水溶液中形成的双电层实验数据进行了对比。结果表明, 当未带电表面上水分子更倾向于氧端朝向构型时, 最大熵对应的表面荷电 (CME) 为负值；此外, 当 $\delta\mu$ 随电位变化时, 形成熵在 CME 附近呈现出明显的非对称性。然而, 该模型无法同时再现来自两项独立实验研究的电容和熵测量结果, 表明模型仍存在不足, 或实验数据中可能存在误差。尽管如此, 本工作强调了在研究双电层时同步测量电容和熵的重要性。

关键词: 双电层; 过剩熵; 形成熵; 界面水; 最大熵荷电